symmetry

MDPI

Article

Study on Water Jet Characteristics of Square Nozzle Based on CFD and Particle Image Velocimetry

Zhuo Fu [1], Kun Li [1], Yongjun Pang [2,*], Liyong Ma [2,*], Zhanying Wang [2,3,*] and Bin Jiang [4]

[1] Department of Mechanical and Electronic Engineering, Changsha University, Changsha 410199, China
[2] School of Mechanical Engineering, Hebei University of Architecture, Zhangjiakou 075051, China
[3] Zhangjiakou Special Equipment Intelligent Monitoring Operation and Maintenance Technology Innovation Center, Zhangjiakou 075051, China
[4] School of Mechanical and Electronic Engineering, Central South University, Changsha 410083, China
* Correspondence: pyj1063@hebiace.edu.cn (Y.P.); maliyong@buaa.edu.cn (L.M.); wzy1293@hebiace.edu.cn (Z.W.); Tel.: +86-133-3303-3990 (Y.P.); +86-189-3263-7968 (L.M.); +86-313-4187755 (Z.W.)

Abstract: Water jet technology is widely used in various fields, in which the nozzle is an important element to form the jet. To solve the problem of low water jet operation efficiency of square nozzles, the internal flow channel structure of the nozzle of the key jet device is studied. Through the combination of computational fluid dynamics (CFD) and particle image velocimetry (PIV) experiments, the influence of main structural parameters such as the contraction angle and length-to-diameter ratio of the inner flow channel on the velocity and length of the constant-velocity core region is explored. Since the jet flow structure is a symmetrical structure along the axial direction, the model of the jet flow structure was built half of the model along the axial direction. The results show that a smaller length-to-diameter ratio and a smaller contraction angle of the nozzle result in better jet cohesion and lower dynamic pressure in the constant-velocity core area, which is more suitable for long-distance, low-pressure water jet operations.

Keywords: water jet; square nozzles; computational fluid dynamics (CFD); particle image velocimetry (PIV); constant-velocity core

check for updates

Citation: Fu, Z.; Li, K.; Pang, Y.; Ma, L.; Wang, Z.; Jiang, B. Study on Water Jet Characteristics of Square Nozzle Based on CFD and Particle Image Velocimetry. *Symmetry* **2022**, *14*, 2392. https://doi.org/10.3390/sym14112392

Academic Editors: Toshio Tagawa and Sergei D. Odintsov

Received: 26 August 2022
Accepted: 7 November 2022
Published: 12 November 2022

Publisher's Note: MDPI stays neutral with regard to jurisdictional claims in published maps and institutional affiliations.

Copyright: © 2022 by the authors. Licensee MDPI, Basel, Switzerland. This article is an open access article distributed under the terms and conditions of the Creative Commons Attribution (CC BY) license (https://creativecommons.org/licenses/by/4.0/).

1. Introduction

Hydraulic excavation [1–4] is the primary mechanized technology to excavate lotus roots from mud fields in China. Its working principle is to use the jet flow via the nozzle to wash the soil to collect the lotus roots. The nozzle is a vital component to form a jet and can be considered as a hydraulic energy converter. Scholars have researched the nozzle of the hydraulic lotus root digger [5,6] since the jet characteristics are closely related to the nozzle structure. Some researchers have conducted studies on the internal structure of the circular nozzle, such as the outlet length of the nozzle, the ratio of length to diameter, the shrinkage angle between the inlet and outlet, and the internal streamline [7–11], but these only achieved a slight improvement.

Through nozzle research, some scholars have found that non-circular nozzles are more effective than standard circular nozzles in some properties, such as uniform water distribution [12–15], jet cohesion [16–18], and stronger impact force [19,20].

Comparing the round, regular triangle, and square nozzle, Liu et al. [2] concluded that the square nozzle has a faster jet speed, a relatively longer constant velocity core, and better cohesion. Hence, it is more suitable for jet-breaking operations under submerged conditions. He [21] demonstrated that the square nozzle has higher transmission efficiency and a better stream concentration; therefore, the water jet via the square nozzle has a more noticeable erosion effect on the depth and volume.

The above studies mostly focused on the influence of different outlet facets on the nozzle jet performance, failing to cover the effects of the inner shape change of a noncircular nozzle on the external flow field of the jet nozzle.

To fill this gap and improve the water jet efficiency, we carried out further research on the square nozzle due to its better cohesion performance than other noncircular nozzles. This study exposes what happens on the external flow field of the jet nozzle with changes in the two main structural parameters, corroborated by a PIV experiment.

The remainder of this paper is divided into five sections. The first section presents the nozzle structure and jet characteristics in detail. In the second one, we propose the calculation model based on CFD. The following section represents the theoretical analysis of the relationship of the external flow field of the jet nozzle and the double structure factors, according to the model proposed. The fourth section presents the PIV experiment and the corroboration of our method. In the last section, we provide a summary of the study.

2. Nozzle Structure and Jet Characteristics

Figure 1 shows the nozzle separated into three sections: the inlet section l_r, contraction section ls, and outlet section l_c. The internal flow channel is a rectangular parallelepiped within the outlet section, and one of the contraction sections is in the shape of a square frustum. The water flows through the square nozzle to form a jet. Hence, the change in structure parameters will directly affect the external jet shape and performance. Specifically, unreasonable structure parameters would result in the nozzle jet not working efficiently. Therefore, it is necessary to choose the proper nozzle geometry.

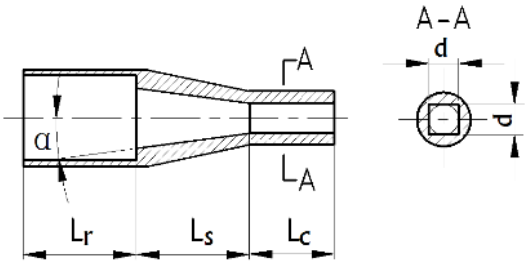


Figure 1. Schematic diagram of a square nozzle structure.

This paper selects the nozzle length-to-diameter ratio and contraction angle as the main parameters researched. The length-to-diameter ratio l_c/d is the outlet length to the diameter of the inscribed circle of the outlet square hole; the contraction angle α is the angle between the generatrix of the circumscribed cone of the constriction section channel and the axis.

In engineering practice, the working medium of the jet is generally liquid, such as air and water. Whether it is submerged or non-submerged, the jet structure is nearly constant. Figure 2 is a schematic diagram of the jet flow structure. According to the hydrodynamic structure characteristics, the water jet is partitioned into four parts: the beginning section, transition section, basic section, and dissipation section.

The beginning section is from the nozzle outlet to the end of the constant-velocity core. The core area flow is constant with the nozzle outlet flow on the velocity and is potential flow, where each point has the same speed and direction. The shear layer, also called the boundary layer, is the area between the jet's inner and outer boundaries in the beginning section. There is a velocity gradient in the shear layer, which generates Reynolds stresses [22], whereby the core area fades away as the spray distance increases. Hence, in Figure 2, plane B is the end of the constant-velocity core and the beginning of the transition section. The transition section is usually omitted in most calculation models since it is too short and complex. The end of the transition section is the threshold plane C, where the basic section begins. In the third section, the distance between the jet outer boundary and

its central axis is b, which grows with the jet distance increase until the jet is completely submerged in the surrounding medium and becomes a static fluid.

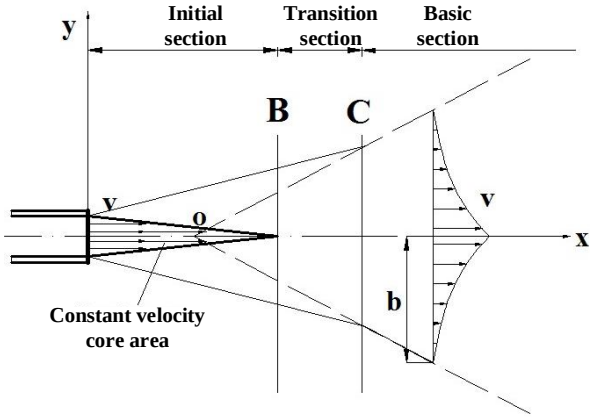


Figure 2. Schematic diagram of jet flow structure.

The speed and length of the constant-velocity core area are critical criteria to evaluate the nozzle jet performance [23]. A greater velocity and a greater length of the core area result in higher nozzle jet erosion and fragmentation efficiency, slower jet attenuation, smaller diffusion, larger volume, and higher efficiency of the jet eroding the soil.

3. Calculation Model Based on CFD

3.1. Governing Equations and Turbulence Model

The jet medium of the square nozzle is water. To simplify the calculation processing, we assume that the fluid is continuously incompressible viscous, and that no heat conduction occurs in the nozzle; therefore, there is no need to solve the energy equation. Equations (1) and (2) are the continuity equation and the N–S equation of incompressible fluid, respectively, to analyze the nozzle jet.

$$\frac{\partial \rho}{\partial t} + \nabla \cdot \left(\rho \vec{v}\right) = 0, \tag{1}$$

$$\rho \frac{d\vec{v}}{dt} = -\nabla \vec{p} + \rho \vec{f} + \mu \Delta \vec{v}, \tag{2}$$

where t is time (ms), v is the fluid velocity (m/s), p is the pressure (MPa), f is the volume force (N/m^3), ρ is the fluid density (kg/m^3), μ is the dynamic viscosity (N·s/m^2), and Δ is the Laplacian.

Since the above control equations are not closed, a new turbulence model must be supplemented to make the equations closed. The realizable k–ε two-equation model was selected as the supplement, seeing that it is more suitable for free flow, channel flow, and boundary layer flow among various turbulence models. The turbulent kinetic energy equation k and the dissipation equation ε are as follows:

$$\frac{\partial}{\partial t}(\rho k) + \frac{\partial}{\partial x_j}(\rho k v_j) = \frac{\partial}{\partial x_j}\left[\left(v + \frac{v_t}{\sigma_k}\right)\frac{\partial k}{\partial x_j}\right] + G_k + G_b - \rho\varepsilon + S_k, \tag{3}$$

$$\frac{\partial}{\partial t}(\rho \varepsilon) + \frac{\partial}{\partial x_j}(\rho \varepsilon v_j) = \frac{\partial}{\partial x_j}\left[\left(v + \frac{v_t}{\sigma_\varepsilon}\right)\frac{\partial \varepsilon}{\partial x_j}\right] + \rho C_1 S\varepsilon - \rho C_2 \frac{\varepsilon^2}{k + \sqrt{\frac{v\varepsilon}{\rho}}} + C_{1\varepsilon}\frac{\varepsilon}{k} C_{3\varepsilon} G_b + S_\varepsilon, \tag{4}$$

where v_t is the eddy viscosity, S_k, S_ε are the user-defined source items, S denotes the average strain rate tensor, the values of C_2 and $C_{1\varepsilon}$ are 1.0 and 1.2, respectively, and the related variables are calculated using the following equations:

$$G_k = \left(-\frac{2}{3}\rho k\delta_{ij} - \frac{2}{3}v\overline{S}_{kk} + 2v_t\overline{S}_{ij}\right)\frac{\partial v_i}{\partial x_j}, C_{3\varepsilon} = \tanh\left|\frac{\mu}{\rho v}\right|, C_1 = \max\left[0.43, \frac{\eta}{\eta+5}\right], \eta = S\frac{k}{\varepsilon}, S = \sqrt{2\overline{S}_{ij}\overline{S}_{ij}}, \overline{S}_{ij} = \frac{1}{2}\left(\frac{\partial v_j}{\partial x_i} + \frac{\partial v_i}{\partial x_j}\right), v_t = C_v\rho\frac{k^2}{\varepsilon},$$
$$C_v = \frac{1}{A_0 + A_s\frac{kU^*}{\varepsilon}}, U^* \equiv \sqrt{S_{ij}S_{ij} + \Omega'_{ij}\Omega'_{ij}}, \Omega'_{ij} = \overline{\Omega}_{ij} - 3\varepsilon_{ijk}\omega_k, A_0 = 4.04, A_s = \sqrt{6}\cos\varphi, \varphi = \frac{1}{3}\cos^{-1}\left(\sqrt{6}W\right),$$
$$W = \frac{2\sqrt{2}S_{ij}S_{jk}S_{ki}}{S^3}, G_b = g_i\frac{v_t}{\mathrm{Pr}_t}\frac{\partial T}{\partial x_i},$$

where v_j is the eddy viscosity, σ_k and σ_ε have the values 1.44 and 1.9, respectively, $\overline{S}_{ij}$ is the average strain rate tensor, Ω'_{ij} is the average rotation velocity tensor, $\overline{\Omega}_{ij}$ is the rotation rate tensor obtained in a rotating coordinate system rotating at angular velocity ω_k, Pr_t is the turbulent Prandtl number of energy, and the g_i value is 0.85.

3.2. Numerical Model and Method

Numerical analysis was conducted using the simulation software FLUENT. To simulate the inner and outer flow fields, we used thick and dense grid nodes to represent the inner part and connected it to a large area representing the external flow field using thin and sparse grid lines. Since the jet flow structure is a symmetrical structure along the axial direction, the model of the jet flow structure was built for half of the model along the axial direction, as shown in Figure 3. The mesh consisted of 343,356 elements and 327,850 nodes. Referring to the boundary conditions, the gravitational acceleration was set to 9.81 m/s^2, and the outer part was designed as a cuboid with a width and height of 0.2 m and a length of 1 m to ensure that the water jet could fully move in the flow field. The average flow rate at the initial position of the inlet was set to 15, the wall was set as an adiabatic wall, and the medium in the flow field was set as water (continuous fluid with low viscosity). It was assumed that the nozzle surface was insulating, that no heat conduction occurred in the nozzle, and that water was the medium in the flow field.

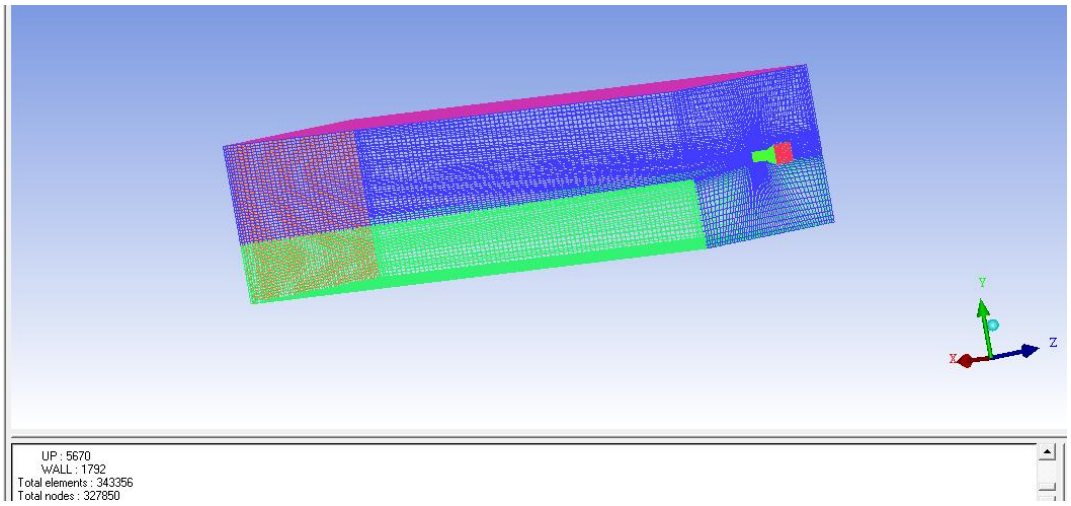


Figure 3. Simulation model of inner and outer flow fields.

4. Analysis of Simulation Results

4.1. Effects of Different Length-to-Diameter Ratios on the Constant-Velocity Core

We measured the size of the nozzles tested, and, in the simulation, related parameters were set as follows: hydraulic diameter, 22.8 mm; inscribed circle diameter of the outlet, 11.4 mm; contraction angle, $\alpha = 13°$; inlet length, 2 mm; average velocity at the initial position of the inlet, 15 m/s. Using these given and fixed parameters, we researched the effect of outlet length on jet efficiency.

From the comparison of jet center velocity along the x-axis (x-velocity) attenuation of nozzles with different length-to diameter ratios in Figure 4, as the length-to-diameter ratio

increases, the jet center velocity at the outlet also increased, where the starting position of the outlet was set as the origin of the horizontal axis.

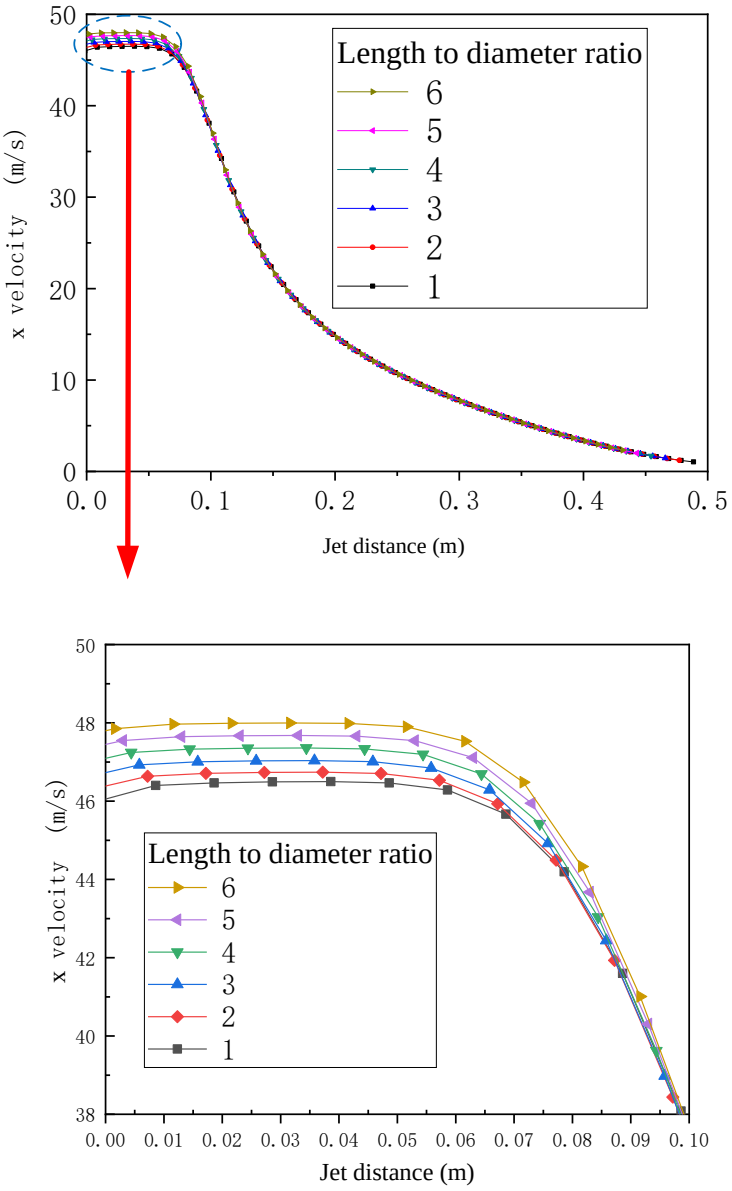


Figure 4. The x-velocity curves as a function of length-to-diameter ratio.

Figure 5 concisely records that the nozzle with a larger length-to-diameter ratio had a shorter jet isokinetic nucleus length. The physical explanation is that a more extended outlet section causes the flow to lose more energy along the way, the jet velocity with a larger length-to-diameter ratio nozzle decreases more quickly, and the constant-velocity core is shorter.

Because these nozzles have the same contraction angle, the energy after the water leaves the contraction section is the same. The length-to-diameter ratio is the main factor that affects the jet velocity and distribution in the outlet.

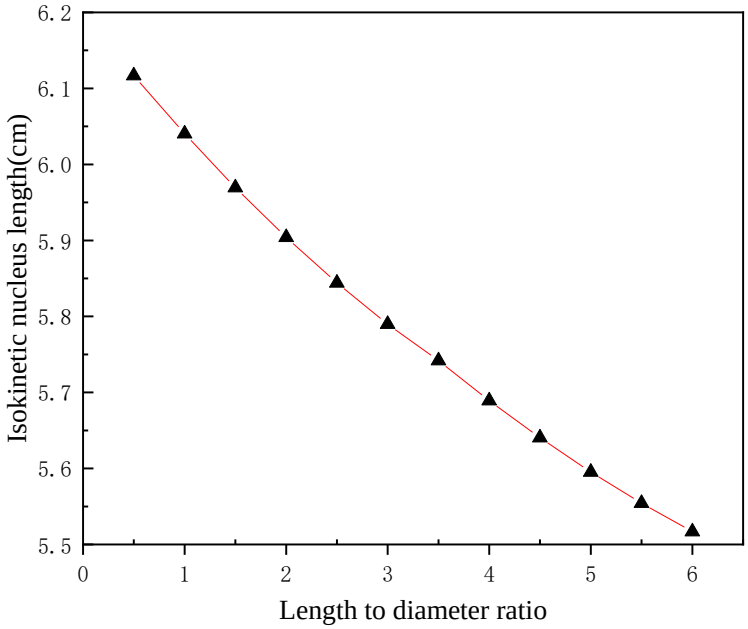
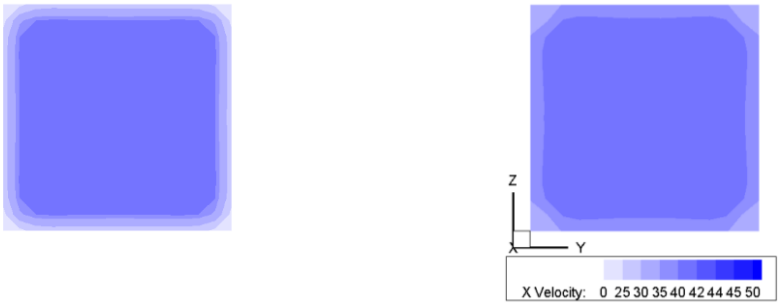


Figure 5. Relationship between isokinetic nucleus length and length-to-diameter ratio.

As shown in Figure 6, Compared with $l_c/d = 1$, the center flow velocity of the nozzle with $l_c/d = 6$ had a bigger value t. However, the flow velocity near the internal surface was smaller when $l_c/d = 6$, and the apex angular velocity decreased. A longer nozzle outlet section resulted in more energy loss, thus further reducing the near-wall liquid rate. This infers that the jet from a nozzle with an excessive length-to-diameter ratio would lose more energy before ejecting, and its velocity would decay more quickly once spewed out. However, the length-to-diameter ratio was positively related to the center flow velocity at the outlet, because, in this section, the flow energy goes from the near-wall to the center, and the longer section distance contributes to more energy transfer.



(**a**) $l_c/d = 1$ (**b**) $l_c/d = 6$

Figure 6. Images of flow velocity at the outlet with length-to-diameter ratios of 1 and 6.

On the basis of the above analysis, we can conclude that the flow via a nozzle with a larger length-to-diameter ratio is faster but loses more energy in the outlet section. After leaving the nozzle, the jet velocity and pressure drop more immediately, and the constant-velocity core is shorter. In contrast, the nozzle with a smaller length-to-diameter ratio has better jet stability and a longer constant velocity core. The smaller-aspect-ratio nozzle demands a higher driving force to meet the same working requirement due to its lower jet velocity and pressure. Therefore, a large length-to-diameter ratio is not suitable for long-distance water jet operations; a small length-to-diameter ratio is more proper for water jet operations requiring longer distance and low pressure.

4.2. Effects of Different Contraction Angles on the Constant-Velocity Core

In this subsection, $l_c/d = 3$, the contraction angle was taken as an independent variable, and the remaining variables were as before. The outlet remained as the abscissa origin.

As illustrated in Figure 7, different contraction angles had similar velocity decay curves; the angle increase promoted a quicker constant-velocity core. Therefore, the flow spewed out more quickly.

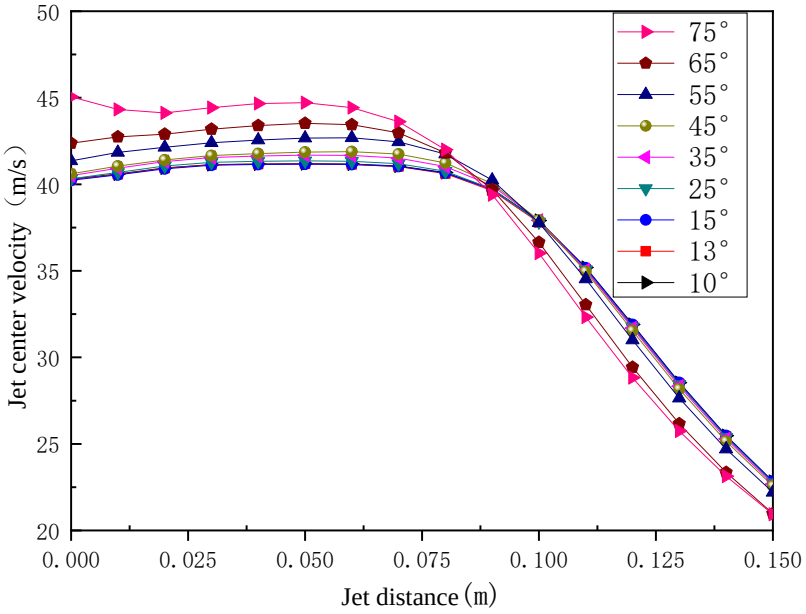


Figure 7. Velocity curves as a function of contraction angle.

In Figure 8, the relationship between isokinetic nucleus length and contract angle describes that when, $\alpha < 60°$, the core length fluctuated within a relatively smaller range; however, when $\alpha \geq 60°$, the length dropped rapidly. The contraction angle was negatively correlated with the length of the contraction section. The fluid flow in the nozzle contraction section and outlet section was turbulent, resulting in its low stability and faster energy dissipation. Therefore, flow with a larger contraction angle enters the basic section earlier, its velocity decreases more quickly, and the constant-velocity core is shorter.

As the nozzle contraction angle increases, the acceleration effect of the liquid flow improves, and the liquid flow velocity in the outlet section increases. After the liquid flow enters the outlet section, the central liquid flow and the near-wall liquid flow continuously exchange energy, the energy of the near-wall liquid flow is continuously transferred to the central liquid flow, and the speed of the central liquid flow gradually starts to increase. Therefore, a larger contraction angle results in a greater center velocity of the liquid flow in the outlet section.

Figure 9a,b show the difference between $\alpha = 10°$ and $\alpha = 75°$. It can be seen in Figure 9 that the nozzle with a contraction angle of 75° had a higher jet center velocity. When the contraction angle was too large, the velocity near the wall decreased. This is because, when the nozzle contraction angle is too large, there is a phenomenon of liquid flow shrinking at the exit of the contraction section. At the exit of the contraction section, a local liquid flow breaks away from the wall and then attaches to the wall. Therefore, when liquid flows close to the wall, speed and energy are lost. Because the jet of a nozzle with an excessively large contraction angle loses more energy in the nozzle, the jet velocity decays more quickly after the liquid flow leaves the nozzle.

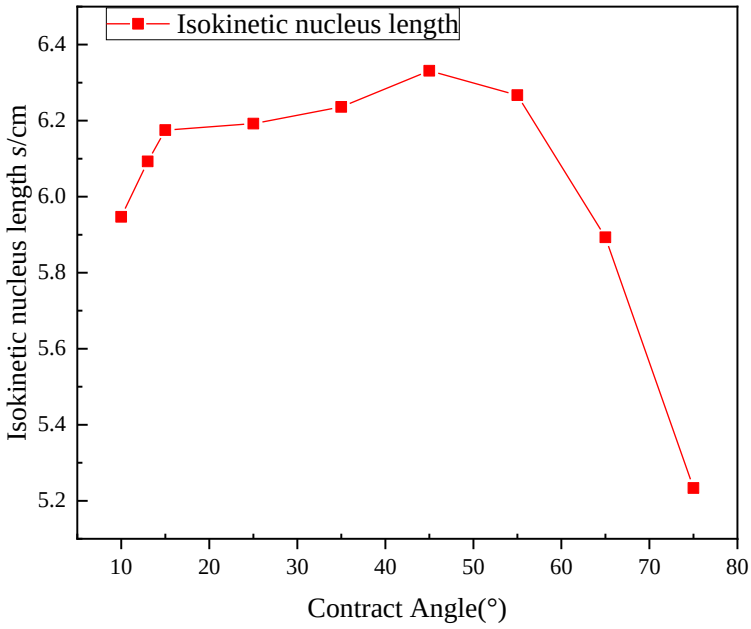
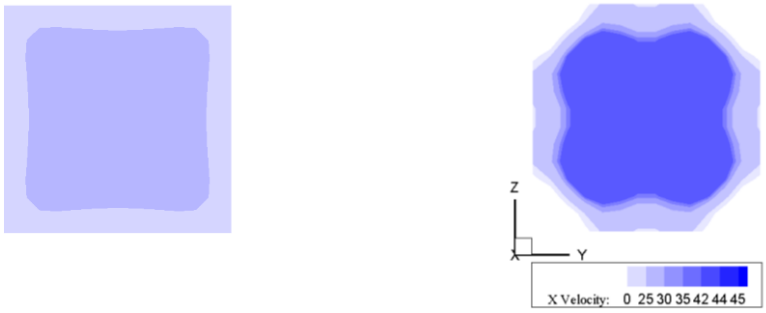


Figure 8. Relationship between isokinetic nucleus length and contract angle.



(**a**) α=10° (**b**) α=75°

Figure 9. Images of flow velocity at the outlet with $\alpha = 10°$ and $\alpha = 75°$.

The center velocity of the liquid flow of a nozzle with a larger contraction angle is relatively larger. However, the stability of the jet is poor. After leaving the nozzle, the speed and pressure of the jet drop more quickly, and the constant-velocity core is shorter. Therefore, nozzles with larger contraction angles are not suitable for long-distance water jet operations. The nozzle with a smaller contraction angle has relatively better jet stability and a longer constant-velocity core. However, the speed and pressure of the jet are relatively small. To achieve the same speed and meet the same working requirements, the nozzle with a small contraction angle needs to work under the condition of greater power, and the energy conversion rate is low.

4.3. Uncertainity Analysis

The simulation in this paper was carried out under absolute ideal assumptions, whereas the following uncertainties may exist in actual engineering:

(1) In actual engineering, the components of sediment are not single; thus, the actual jet velocity and angle may be affected by the fluid composition;
(2) The temperature change was not considered in the simulation, whereas, in actual engineering, the jet flow variable is affected by the ambient temperature; thus, the uncertainty of temperature should be considered in the experiment;
(3) The wear of the nozzle was not considered in the simulation; however, in an actual project, the wear of the nozzle affects the jet.

5. Experiment

Particle image velocimetry (PIV) was employed to experiment with different square nozzles. Figure 10 shows the experimental device of the PIV speed measurement system, which consists of two parts, i.e., the waterway system and the measurement system. One end of the water pump pumps water from the water tank that was put into the tracer particles, while the other end of the water pump is connected to the nozzle that was fixed in the glass cylinder through a pipeline. The laser light generated by the laser transmitter passes through the sheet light source to form a sheet light area. When the sheet light area coincides with the position of the flow field area to be measured, the CCD camera is perpendicular to the measurement watershed for shooting.

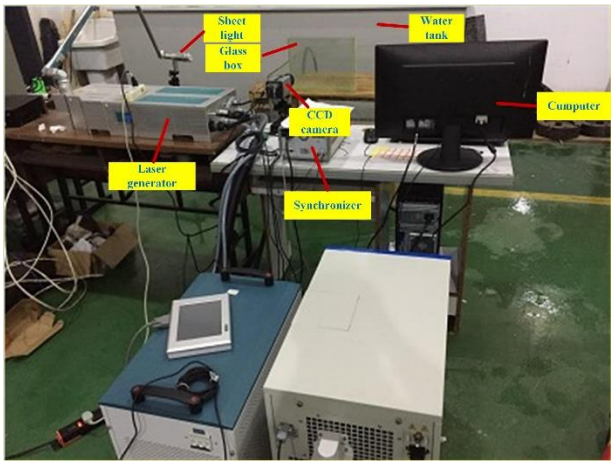


Figure 10. Experimental devices.

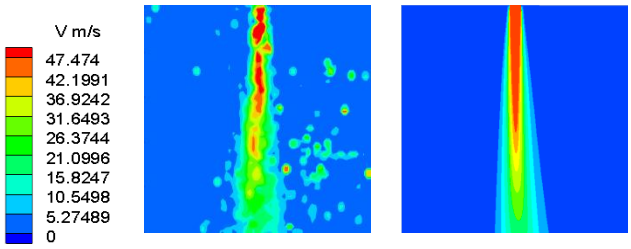
The measurement of the nozzle jet velocity field in the experiment was a two-dimensional PIV measurement experiment, and the workbench INSIGHT4G system was used for image acquisition. The software TECPLOT converted the velocity information of each tracer particle in each picture into the overall velocity field cloud image.

Figure 11a–c show that the experiment and simulation results were nearly the same in the velocity distribution, the constant-velocity core, and the velocity at the exit, regardless of whether $l_c/d = 2$ or $l_c/d = 3$. Table 1 again demonstrates that there were only tiny errors between the two results. Furthermore, the jet was faster in $l_c/d = 3$ than in $l_c/d = 2$, which is consistent with the conclusion of the model analysis.

Table 1. Outlet jet velocities at $l_c/d = 2$ and $l_c/d = 3$.

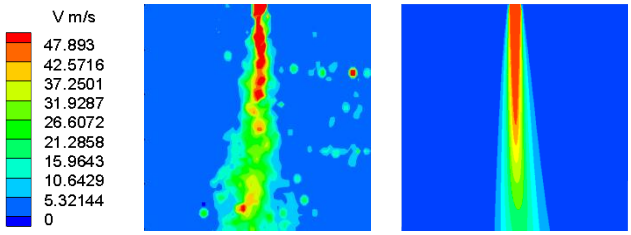
I_C/d	Outlet Jet Velocity (m/s)	
	Experimental Value	Simulation Value
2	47.474	47.53
3	47.893	47.55

Figure 12 shows that the experimental velocity field was almost consistent with the simulated velocity field, and the jet velocity attenuation was similar. Figure 12a,c indicate that the maximum jet velocity with a contraction angle of 45° was greater than that with a contraction angle of 13°, which is also in line with the conclusion of the numerical simulation. Table 2 shows that, in the practical velocity field, the outlet jet velocity at $\alpha = 45°$ was higher than that at $\alpha = 13°$; the error between the experimental and simulation results was small, and the velocity field distributions were virtually consistent.



(**a**) Experimental velocity field, $l_c/d=2$

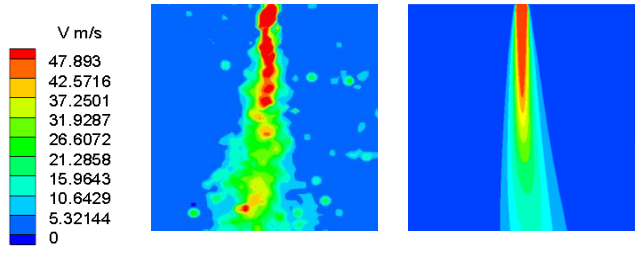
(**b**) Simulation velocity field, $l_c/d=2$



(**c**) Experimental velocity field, $l_c/d=3$

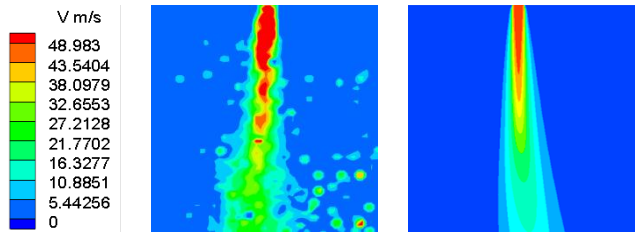
(**d**) Simulation velocity field, $l_c/d=3$

Figure 11. Comparison of experiment and simulation results with different length-to-diameter ratios.



(**a**) Experimental velocity field $\alpha=13°$

(**b**) Simulation velocity field, $\alpha=13°$



(**c**) Experimental velocity field, $\alpha=45°$

(**d**) Simulation velocity field, $\alpha=45°$

Figure 12. Comparison of experiment and simulation results with different contraction angles.

Table 2. Outlet jet velocities at $\alpha = 13°$ and $\alpha = 45°$.

α	Outlet Jet Velocity (m/s)	
	Experimental Value	**Simulation Value**
13°	47.893	47.55
45°	48.98	48.74

In summary, the PIV experiment and simulation had approximate results, including similar jet velocity attenuation, almost consistent constant-velocity cores, and jet velocity with negligible errors. These results show that the numerical simulation scheme was effective.

6. Conclusions

In this paper, numerical simulations and experimental tests are carried out for the jet flow field of square nozzles with different length-to-diameter ratios and contraction angles; the results were analyzed, and the conclusions are as follows:

(1) The particle image velocimetry experiment verified the validity of the simulation scheme based on the realizable turbulence model.
(2) A larger length-to-diameter ratio of a square nozzle results in a longer flow energy exchange distance, greater flow deceleration, and greater velocity in the constant-velocity core area.
(3) A larger constriction angle of the square nozzle results in a better acceleration effect of the liquid flow in the constriction section, increased velocity when entering the outlet section, and greater velocity in the isokinetic core region. Therefore, when the water jet impact crushes and removes soil above the lotus root, the design shrinkage angle of the square nozzle used should not be greater than 60°; the appropriate shrinkage angle is $\alpha = 45°$.

Author Contributions: Conceptualization, Z.F. and K.L.; methodology, L.M. and Y.P.; software, B.J. and L.M.; validation, Z.F., K.L., and Z.W.; formal analysis, L.M.; investigation, Z.F. and L.M.; resources, Z.F. and B.J.; data curation, Z.F.; writing—original draft preparation, Z.F. and B.J.; writing—review and editing, L.M., Z.W. and B.J.; supervision, K.L., Z.W., and Y.P.; project administration, Z.F., K.L., L.M. and Y.P.; funding acquisition, Z.F., K.L., L.M. and Y.P. All authors read and agreed to the published version of the manuscript.

Funding: This work was supported by the project of Changsha Municipal Natural Science Foundation (grant number kq2007085), the Basic Scientific Research Business Project of Hebei University of Architecture (grant number 2022QNJS02), the Basic Scientific Research Business Project of Hebei University of Architecture (grant number 2021QNJS08), the Outstanding Youth Project of Education Department of Hunan Province, China (grant numbers 20B068 and 20C0168), the Chinese 14th Five-Year Plan Project of Hebei Higher-Education Association (grant number GJXH2021-109), and the Education and Teaching Reform Research and Practice Project of Hebei University of Architecture (grant number 2022JY125).

Data Availability Statement: The data presented in this study are available on request from the corresponding authors.

Conflicts of Interest: The authors declare no conflict of interest.

References

1. Liu, M.C.; Mao, D.W.; Wang, Z.H.; Song, Z.H.; Wang, G.R.; Li, F.D. Research Status of Lotus Root Digging Technology and Prospect of Lotus Root Harvesting Technology in Yellow Kiver Delta Region. *Agric. Eng.* **2018**, *8*, 1–5.
2. Liu, Y.; Ke, W.; Huang, X. Lotus rhizome's manual and mechanical excavations. *J. Chang. Veg.* **2014**, *21*, 10–15.
3. Guo, Y. Design and research of Lotus rhizome excavator for paddy field. Master's Dissertation, Huazhong Agricultural University, Wuhan, China, 2015.
4. Zhang, Y.; Jiang, Z. Development of jet-type lotus-digging machine. *Grain Oil Process. Food Mach.* **1982**, *8*, 33–38.
5. Jing-Fei, H.E.; Chen, J.G.; Wang, A.L.; Zhang, Y.Y. Study on Flow Field of a New Digging Lotus Based on the Vortex Theory. *Comput. Simul.* **2015**, *32*, 184–187.
6. Wu, H.; Xia, J.; Zhang, G.; Wang, P.; Lao, S.; Zhang, X. Design and Experiment of Spin-jet Flow Type Lotus Root Digging Machine based on EDEM-Fluent. *Trans. Chin. Soc. Agric. Eng.* **2018**, *34*, 9–14.
7. He, F.; Xie, J.; Yang, J. Effect of Nozzle Geometry on Aerodynamics of Free Jet. *Chin. J. Appl. Mech.* **2001**, *18*, 114–119.
8. Vasil'Ev, O.A.; Minin, S.N.; Shipovskikh, A.V. Investigation of the Flow Structure in Nozzles with a Throat Section of Constant Height. *Fluid Dyn.* **1990**, *25*, 944–949. [CrossRef]
9. Etzold, M.; Deswal, A.; Chen, L.; Durst, F. Break-up Length of Liquid Jets Produced by Short Nozzles. *Int. J. Multiph. Flow* **2018**, *99*, 397–407. [CrossRef]

10. Geng, L.; Hu, Z.; Lin, Y. Numerical Investigation of the Influence of Nozzle Geometrical Parameters on Thrust of Synthetic Jet Underwater. *Sens. Actuators A Phys.* **2018**, *269*, 111–125. [CrossRef]
11. Liu, P.; Zhang, D. Research on Calculation of the Influence of Nozzle Geometric Parameters on the Property of Efflux Flow Field. *J. Mach. Des.* **2017**, *24*, 50–52.
12. Chen, C.; Yuan, S.; Li, H.; Wang, C. Effect of Non-circle Nozzle on Hydraulic Performance of Impact Variable-rate Sprinkler. *Trans. Chin. Soc. Agric. Mach.* **2011**, *42*, 111–115.
13. Wei, Y.; Yuan, S.; Li, H.; Xiang, Q.; Chen, C. Hydraulic Performance Experiment of the Variable-rate Sprinkler with Non-circle Nozzle. *Trans. Chin. Soc. Agric. Mach.* **2011**, *42*, 70–74.
14. Jiang, Y.; Hong, L.I.; Xiang, Q.J.; Chen, C. Experimental Study on Breakup Length and Range of Free Jet for the Non-circle Jet Nozzle. *J. Irrig. Drain.* **2014**, *33*, 149–153.
15. Hua, L.; Jiang, Y.; Hong, L.I.; Zhou, X. Hydraulic Performance of Low Pressure Sprinkler with Special-shaped Nozzles. *J. Drain. Irrig. Mach. Eng.* **2018**, *36*, 1109–1114.
16. Li, X.; Chen, M.; Wang, Y.; Hu, J.; Sun, Z.; Christopher, D.M.; Cheng, L. Measurements of Concentration Decays in Underexpanded Jets through Rectangular Slot Nozzles. *Int. J. Hydrogen Energy* **2018**, *43*, 9884–9893. [CrossRef]
17. Liu, J.; Lv, H.; Wang, L. Performance of Internal Flow Field of Shaped Nozzle with the High-pressure Water Jet Cleaning Equipment. *Mach. Build. Autom.* **2015**, *44*, 65–67.
18. Liu, J.; Wang, A.; Cai, J.; Jiang, B. Comparison of Water Jet Flow Field Between Non-Circle Nozzles and Conical Nozzles. *Light Ind. Mach.* **2019**, *37*, 19–24.
19. Zhao, X. Experimental Study on Jet Characteristics of Abnormity Nozzle. Master's Dissertation, Tianjin University of Science and Technology, Tianjin, China, 2005.
20. Huang, K.L.; Yang, Y.X.; Wen, Q.; Huang, K.H.; Jian, Z.; Li, Z.B. Analysis about Influence of PDC Rectangular Nozzles on Bottom Flow Field. *Mech. Res. Appl.* **2012**, *25*, 28–30.
21. He, X. *Numerical Simulation and Experimental Study of Self-Oscillating Pulsed Nozzles with Different Nozzle Shapes*; Hunan University of Technology: Zhuzhou, China, 2014.
22. Hoyas, S.; Sendín, J.J. Reynolds number effects on the Reynolds-stress budgets in turbulent channels. *Phys. Fluids* **2008**, *20*, 133. [CrossRef]
23. Xiong, J.; Liao, R.; Chen, X. *Rock-Breaking Theory and Technology of Jet-Assisted Drilling*; Sichuan Science and Technology Press: Chengdu, China, 2007.